

FEDSM-ICNMM2010-300' -

THREE-DIMENSIONAL AERODYNAMIC OPTIMIZATION FOR AXIAL-FLOW COMPRESSORS BASED UPON THE INVERSE DESIGN AND THE AERODYNAMIC VARIABLES

Liu He Peng Shan

School of Jet Propulsion
Beijing University of Aeronautics and Astronautics
Beijing 100191, P. R. China

Email: heliu282@163.com

Email: PShan@buaa.edu.cn

ABSTRACT

Integrating a genetic algorithm code with a response surface methodology code based upon the artificial neural network model, this paper develops an optimization system. By introducing a quasi-three dimensional through-flow design code and a design code of axial compressor airfoils with camber lines of arbitrary shape, and involving a three-dimensional computational fluid dynamics solver, this paper establishes a numerical aerodynamic optimization platform for the three-dimensional blades of axial compressors. The optimization in this paper mainly has four features. First, it applies the conventional inverse design method instead of the common computer aided design parameterization method to generate a three-dimensional blade. Second, it chooses aerodynamic parameters with physical meaning as optimization design variables instead of purely geometrical parameters. Third, it presents a stage-by-stage optimization strategy about the multistage turbomachinery optimization. Fourth, it introduces the visual sensitivity analysis method into optimization, which can adjust variation ranges of variables by analysing how great the variables influence the objective function. The above techniques were applied to the redesign of a single rotor row and two double-stage axial fans separately. The departure angles and work distributions in the inverse design were taken as design variables separately in optimizations of the single rotor and double-stage fans, and they were parametrically represented by means of Bézier curves, whose parameters were used as the optimization variables in the practical operation. The three investigated examples elucidate that not only the techniques mentioned above are appropriate and effective in engineering, but also the design guidance for similar inverse design problems can be obtained from the optimization results.

NOMENCLATURE

c Absolute velocity

C_p	Static pressure rise coefficient = $\frac{P - P_1}{\rho_{inlet} U_{tip}^2 / 2}$
\dot{m}	Mass flow rate
o	ANN actual output vector
P	Static pressure
P	Total pressure
t	ANN expected output vector
T	Total temperature
U	Uniform Design
U	Rotor linear speed
w	Relative velocity
z, r, ϕ	Cylinder coordinates
β_b	Angle between camber line and axial direction
Φ	Flow coefficient = c_z / U_{tip}
τ	Work coefficient = $(U_2 c_{2u} - U_1 c_{1u}) / U_2^2$
Ω	Degree of reaction = $\frac{1}{2} (w_1^2 - w_2^2) / (U_2 c_{2u} - U_1 c_{1u})$
η	Adiabatic efficiency = $\left[(P_2 / P_1)^{\frac{\gamma-1}{\gamma}} - 1 \right] / (T_2 / T_1 - 1)$
σ	Total pressure recovery coefficient = P_2 / P_1
π	Total pressure ratio
ρ	Static density

Subscripts

1,2	Inlet, outlet of rotor/stator/compressor
<i>inlet</i>	Inlet of compressor
r, u, z	Radial, tangential, axial components
<i>tip</i>	Blade tip

Abbreviation

ANN	Artificial Neural Network
BP	Back Propagate
CAD	Computer Aided Design

CFD	Computational Fluid Dynamics
DOE	Design of Experiment
GA	Genetic Algorithm
I_{\max}	Number of maximum cycles
LE, TE	Leading edge, trailing edge
NURBS	Non-uniform rational B-spline
RMSE	Root mean square error = $\sqrt{\sum_{i=1}^l (o_i - t_i)^2 / l}$
Rotor1	Rotor of first stage
RSM	Response Surface Methodology
SEQV	Von Mises stress
Stage1	First stage of compressors
Stator1	Stator of first stage

1 INTRODUCTION

Aerodynamic design methods for turbomachinery blades have passed a long process of development. In order to improve the design or off-design performance, shorten the design cycle, and reduce both cost and dependence on design experience, the numerical optimization algorithms have been introduced into the field of turbomachinery design. With the development of CFD and the great improvement of parallel computing technology over the last decade, the numerical optimization based on CFD simulation is becoming more popular than ever.

In terms of the complexity of optimization objects, up to date there have been many optimizations about two-dimensional cascades (Pierret and Van den Braembussche [1]), quasi-three dimensional blades (Chung *et al.* [2]) and three-dimensional single rotor or stator rows (Kim *et al.* [3], Bartold and Joos [4]). Except for some fans and pumps, few turbomachines operate as the isolated blade row. So it is of more practical significance to perform a single-stage optimization involving two rows or a multistage optimization. In the recent few years papers on the study of the single-stage optimization (Öksüz and Akmandor [5], Bonaiuti and Zangeneh [6], Arabnia and Ghaly [7]) and even the multistage optimization (Wang *et al.* [8], Chen and Yuan [9]) have been published. Arabnia *et al.* [7] used GA and ANN model to redesign a single-stage axial turbine for multiple operation point optimization. Wang *et al.* [8] applied the adjoint method to redesign a transonic axial compressor stage and a three-stage axial compressor with the inlet guide vane, formatting blades by using Hicks-Henne functions to parameterize perturbations to an existing blade shape. Evaluating also with multiple operation points, Chen and Yuan [9] used a software iSIGHT to redesign first three blade rows of an axial compressor. Furthermore, there are applications of optimizing a single rotor or stator row to improve the overall performance of a single-stage or multistage compressor (Veress and Van den Braembussche [10]).

In terms of the blade parameterization method, it can be classified into three categories. The first is the CAD method, which parameterizes the surface coordinates of a blade, mostly by means of techniques about free form curves and surfaces, such as the Bézier function (Kim *et al.* [3], Arabnia *et al.* [7]), the B-spline function (Bartold *et al.* [4]), the NURBS function (Chen *et al.* [11], Briasco *et al.* [12]), etc. The second is based on the

conventional inverse design method of turbomachines (Bonaiuti *et al.* [6], Chen *et al.* [13]), which parameterizes the control variables for generating a blade geometry, such as the camber line, the stacking axis, the thickness distribution, etc. This method often combines with techniques about through-flow design and blade formatting design. This method is characterized by choosing aerodynamic parameters as design variables. The primary advantages of the inverse design method are the closer correlations between design parameters and the aerodynamic flow field, and then a more direct control of aerodynamic performances. The third is a combination of the above two methods (Verstraete *et al.* [14]). All of the three methods can choose geometrical parameters as design variables. Chen *et al.* [13] used the multi-section blade parameterization technique, that was to transfer the profile coordinates of several sections into a set of important blade design parameters, such as the stagger angle, the maximum thickness and its location, etc, and then to rebuild the 3D blade. This technique was applied to redesign the NASA Rotor 37. Bonaiuti *et al.* [6] applied a commercial software TURBODESIGN¹ for the inverse design method to redesign a single-stage axial compressor. The design variable was the work distribution. Verstraete *et al.* [14] not only used the Bézier function to parameterize the meridional channel contour and element camber lines, but also selected several important blade formatting parameters to optimize both flow and stress of a small radial compressor impeller.

The review of literatures on 3D turbomachinery optimization elucidates three technical features. First, the design variables are mostly the purely geometrical parameters instead of the aerodynamic parameters. Second, quantities of studies focus on optimizing single blade row. Third, it is lack of a general strategy to perform multistage optimizations. These are parts of the research motivations for the present paper. The optimization here mainly has four features. First, it applies the inverse design method that combines with through-flow design and blade formatting design to generate a 3D blade. Second, it chooses the aerodynamic parameters as design variables. Third, it presents a stage-by-stage optimization strategy for the multistage turbomachinery optimization. Fourth, it introduces the visual sensitivity analysis method into the optimization process. An optimization platform of 3D axial compressor blades with the above techniques is coded by this paper. With the redesign examples of a single rotor row and two double-stage axial fans separately, the capability of these techniques to perform aerodynamic optimizations of both 3D blades and stages is presented.

2 OPTIMIZATION METHODOLOGY

2.1 Optimization Platform

Integrating a GA code with a RSM code based on the ANN model, this paper develops an optimization system. By introducing a through-flow design code and a design code of axial compressor airfoils with camber lines of arbitrary shape (Frost and Wennerstrom [15]) into the system, and involving a commercially available CFD software NUMECA for a fully 3D steady compressible viscous flow, this paper establishes a

numerical aerodynamic optimization platform for 3D axial compressor blades of the single row, single-stage dual rows, or multistage multi-rows. The flow chart of the platform is shown in Fig. 1. It includes mainly seven modules, the Uniform Design code, the ANN model code, the GA code, the BP code, the quasi-three dimensional through-flow design code, the blade formatting design code and the CFD software.

As shown in Fig. 1, a cycle method with its Optimization Check Point is implemented during the optimization process. It adds one design variable point with its CFD simulated objective function value as a new sample into the sampling database, and then starts another cycle. The setting value of the maximum cycle number I_{max} is a compromise between the computing time and the optimization quality.

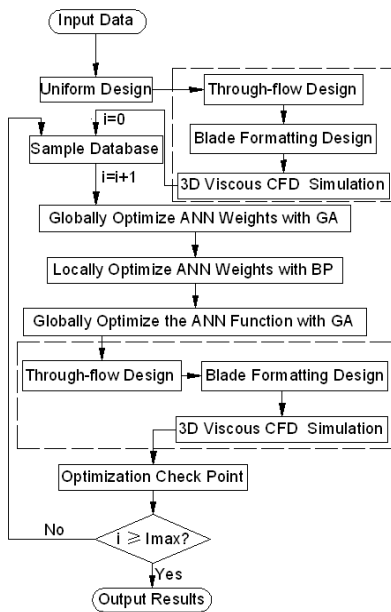


Fig. 1 The flow chart of the optimization platform

2.2 Design Variable Parameterization Setting

The discussion in Section 2 is illustrated by one of this paper's examples, Case 1 of the two-stage fan if no extra explanation. The design variable in this example is the work distribution $c_u r$ used in the through-flow design. There are totally six computing stations along the streamwise direction and eleven $c_u r$ curves along the spanwise direction in each blade row of the two-stage fan in the through-flow design (see Fig. 2). During the optimization process, the following parameterization setting method for $c_u r$ is used. First, to reduce the number of design variables, to simplify the optimization issue and to guarantee no generation of a wiggly blade geometry, four $c_u r$ curves each blade, which are the 1st, 4th, 8th, 11th curves from hub to tip, and six data stored sites on each $c_u r$ curve are chosen (see Fig. 3). Then, each chosen $c_u r$ distribution curve is parameterized by means of the third-order Bézier function. Finally, the change quantities $\Delta c_u r$ with respect to the original

values on the four chosen curves are interpolated by means of the cubic spline to the rest of eleven curves to modify the $c_u r$ distributions of the whole mean cambers, which gives a re-generated blade and guarantees the surface smoothness of it.

The $c_u r$ value at the rotor TE or stator LE is used to normalize those $c_u r$ values on the same curve. The control parameters used to describe the Bézier curve with four control points are shown in Fig. 4. There are four control parameters per Bézier curve, lengths $d1$, $d2$ and angles $\alpha1$, $\alpha2$, and only the values of $\alpha1$, $\alpha2$ change in optimization. So there are only two optimization variables per $c_u r$ curve, and namely eight optimization variables per blade.

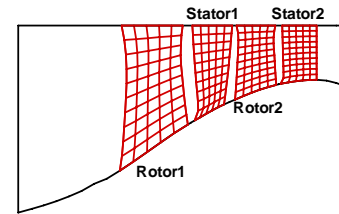


Fig. 2 The $c_u r$ discrete points in the through-flow design

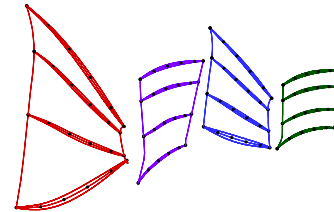


Fig. 3 The data sites of each chosen $c_u r$ curve of all blades

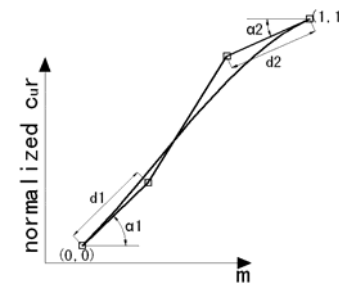


Fig. 4 The control parameters of the Bézier curve of $c_u r$

2.3 Numerical Simulation

In this paper, grids of the two-stage fan are automatically generated by the AutoGrid module of NUMECA. The HOH-type topology structure is applied. The total numbers of grid points of four blocks are 263918, 221445, 226206 and 204402 respectively. The ratio of the Butterfly-type tip clearance to the blade span height is about 0.45% in rotors while there is no clearance in stators. Grid clustering is imposed close to blades and walls in order to have a $y^+ \leq 1$. Grid independence has been tested in the original design. Here in the optimization process for calling CFD solver, the same grid setting parameters are used. An example of

computational grids of the two-stage fan is shown in Fig. 5. To make display legible, one of every two mesh points is shown in three directions. The module Fine of NUMECA is applied to perform CFD simulation. The space discretization is based on a cell-centered finite volume scheme and the system of governing equations is advanced in time using the explicit four-stage Runge-Kutta scheme. Implicit residual smoothing, local time stepping, and multigrid technique are used to reduce the computing time. In the simulation, the one-equation model of Spalart-Allmaras is used for the turbulence closure. CFL number is set to 3. Boundary conditions are imposed on the solid walls, on the period boundaries, at the inlet (total pressure, total temperature, circumferential flow angle and radial flow angle), at the outlet (static pressure) of the computational domain. Furthermore, the mixing plane approach (Denton [16]) is used to set the boundary conditions at the grid interfaces between blocks.

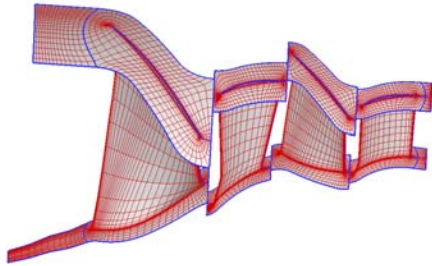


Fig. 5 The CFD grids of the two-stage fan

2.4 Multistage Compressor Optimization Strategy

With regard to the multistage compressor optimization, if multistage multi-rows are optimized integrally, the number of design variables multiplies as the number of stages increases. Then to guarantee the approximation fidelity of the ANN model, it is necessary to increase the number of hidden-layer neurons. Thus not only the training time increases, but also the approximation fidelity is not always good. As a result, it can affect the efficiency and quality of optimization.

Taking the two-stage axial fan for example, this paper proposes a stage-by-stage optimization strategy for the multistage compressor optimization. First, starting from the original design, this paper chooses the relevant design parameters of the rotor and stator of the first stage as design variables, and keeps the parameters of the second stage unchanged. Namely, one multistage optimization is solved based on the change of the whole of the first stage, which is called the first stage optimization. Then, continuing from the optimal configuration after the first stage optimization, this paper chooses the relevant design parameters of the rotor and stator of the second stage as design variables, and keeps the parameters of the first stage unchanged. Namely, another multistage optimization is solved based on the change of the whole of the second stage, which is called the second stage optimization. What needs to be stressed here is that in this stage-by-stage optimization strategy, although only one stage is changed in each stage optimization, the objective function is calculated based on the integral performance of the multistage compressor. This multistage

compressor optimization strategy can greatly reduce the number of design variables. What is more important, it can make the rotor and stator optimized simultaneously and efficiently, when noticing that due to the greatest flow angle between a rotor and a stator, the flow field there has the strongest aerodynamic correlation. So this strategy is apparently different from both the row-by-row optimization strategy and the multistage integral optimization strategy.

Further with regard to one single stage compressor optimization, there are still various treating ways. Take the optimization based on the work distribution as an example again. The first method is just to change $c_u r$ on all computing stations of the single rotor or stator row. This method essentially belongs to the single row optimization. The second method is to change $c_u r$ on the inner computing stations of the rotor and stator at the same time, but to fix $c_u r$ at their LE and TE. Because this method confines the search of the matched feasible solutions in optimization to a relatively small range, it can be called the conservative stage optimization. The third method is to change $c_u r$ on all computing stations of the rotor and stator at the same time. There would be more feasible solutions which meet constraints than the second method. This method can be called the complete stage optimization. The primary characteristics of the latter two methods are, first to couple the flow field changes of the rotor and stator, second to evaluate only the effect of the reasonable stage change on the objective function. In this paper the conservative stage optimization is used.

2.5 Visual Sensitivity Analysis

DOE applied in this paper is the Uniform Design, which falls into two successive phases, the analyzing phase and the sampling phase. The analyzing phase is executed using the visual sensitivity analysis method when the variation ranges of variables are relatively small. Its purposes are to find out the impact and rule of each variable on the objective functions, and then to adjust the variation ranges of variables in the succeeding sampling phase. The purpose of the sampling phase is to make the sampling points distribute as evenly and much as possible in the whole variation ranges. The two phases use different Uniform Design tables $U_n(q^s)$, in which n , q and s is respectively the number of experiments, the number of levels and the number of factors. In Case 1 and 2 of the two-stage fan, they both take $U_{32}(4^{16})$ with 32 tests for the analyzing phase and $U_{30}(30^{16})$ with 30 tests for the sampling phase.

Figure 6 reports that in the analyzing phase, the variation trends of the average of the target sum of the objective function versus factors, i.e. variables, in the 1st stage optimization of Case 1. The range of all levels of the same factor is defined as the difference between the largest value and the smallest one of this factor. For example the vertical coordinate interval of two dashed lines in Fig. 6 a) is the range of the variable 7, i.e. V7. The range can reflect the impact of factors on a target. In order to guarantee that there is no irrational blade configuration, the variable variation ranges in the analyzing phase are relatively small one in

general. After the visual sensitivity analysis, the variation ranges of variables, which have a greater impact or whose extrema locate at one end, can be moderately enlarged.

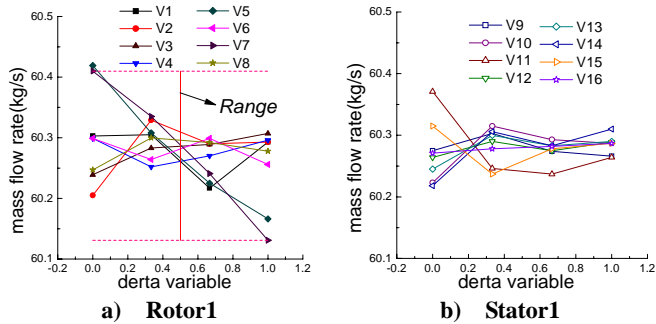


Fig. 6 The variation trends of the average of the target sum of the objective function versus variables in the 1st stage optimization of Case 1 of the two-stage fan

3 SINGLE BLADE ROW OPTIMIZATION

3.1 Description of the Case

An additional zero-stage compressor rotor of a small turbojet engine (Liu *et al.* [17]) serves as the first optimization example. This case took the peak efficiency operation point of the original design of the rotor at the 100% speed as the optimization condition. Namely during the optimization process, the static pressure at the outlet was equal to that of the original design. The optimization objective was to achieve the maximum adiabatic efficiency of the rotor. In this case the departure angles on the mean camber lines in the blade formatting design were taken as the design variables. Three camber lines of departure angle distributions respectively on the hub, middle and tip of the rotor with six data access sites each were chosen. Generating a new blade here just needed to call the blade formatting code while the through-flow design code was not used (see Fig. 1). In order to keep the through-flow and compression capacities of the rotor unchanged, the optimization constraints were to keep the differences between \dot{m} , π and their original values less than 0.5% of the latter. As shown in Fig. 7, the departure angle distribution curve was parameterized by means of the third-order Bézier function. This case chose five optimization variables per Bézier curve, which were the X-coordinates and Y-coordinates of the 2nd, 3rd control points, and the Y-coordinate of the 4th control point. As also seen from Fig. 7, the departure angle at the LE and TE was separately equal to the incidence angle and the deviation angle. Namely during the optimization process the deviation angle changed while the incidence angle kept fixed. So there were a total of 15 optimization variables in the practical operation. The other treating methods were similar to those of the work distribution parameterization setting as mentioned above. I_{\max} was set to 50.

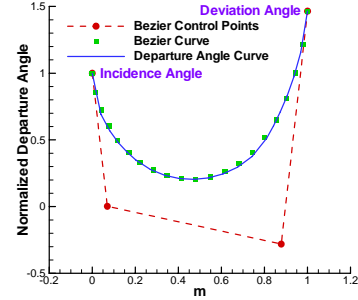


Fig. 7 The distribution curve, the control points and Bézier curve of the normalized departure angles on the rotor hub camber line

3.2 Optimization Process

Figure 8 reports the optimization process for the maximization of the rotor efficiency. In each optimization cycle there is one variable point evaluated to have the maximum efficiency and obtained by optimizing the ANN model function with GA. The three lines in Fig. 8 separately correspond to the evaluated maximum efficiency value, the CFD efficiency value corresponding to the above variable point, and the maximum CFD efficiency value among this point and all points in the sample database.

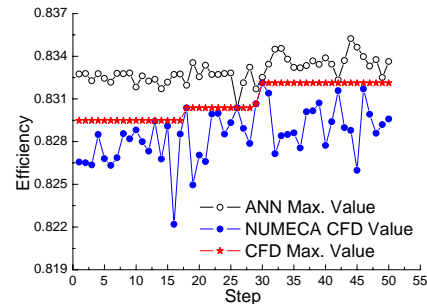


Fig. 8 The optimization process for the maximization of the rotor efficiency

3.3 Results and Analysis

Figure 9 reports the comparison of the hub, middle, tip departure angle distribution curves before and after optimization. The departure angles at the hub change greatly. Figure 10 shows the comparison of the radial projections of the rotor hub, middle, tip element airfoils before and after optimization.

The comparison of the rotor performances at the peak efficiency point before and after optimization is reported in Table 1. η of the optimal rotor gains 0.73 percentage points while \dot{m} is about up by 0.05% and π is about down by 0.11%, that meet the specified constraints. The comparison of the C_p distributions at the 10%, 90% span of the rotor at the peak efficiency point is shown in Fig. 11. First, the normal shock at the tip moves downstream and is stretched to a weaker one. Second, in Fig. 10 the optimal tip airfoil presents a configuration similar to that of the S-shape supersonic precompression airfoil, and in Fig. 11, a noticeable corresponding pressure distribution is also presented. Third, the rotor work loading moves downstream.

Table 1 Comparison of the rotor performances at the peak efficiency point

	Original	Optimal	Increment
\dot{m} (kg/s)	7.921	7.925	0.05%
π	1.430	1.428	-0.11%
η	0.8248	0.8321	0.73 percentages

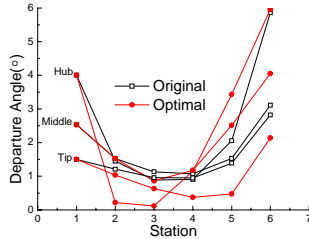


Fig. 9 Comparison of the rotor departure angle distributions

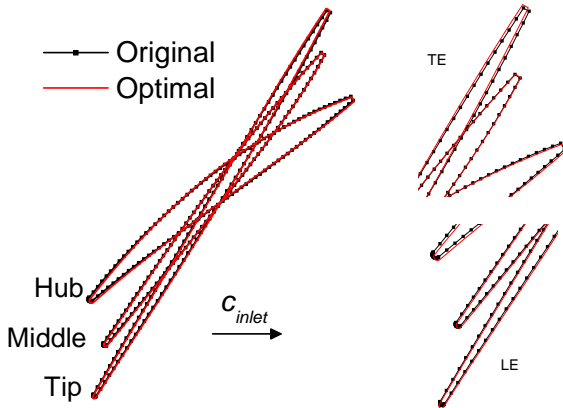


Fig. 10 Comparison of the rotor hub, middle, tip element airfoils

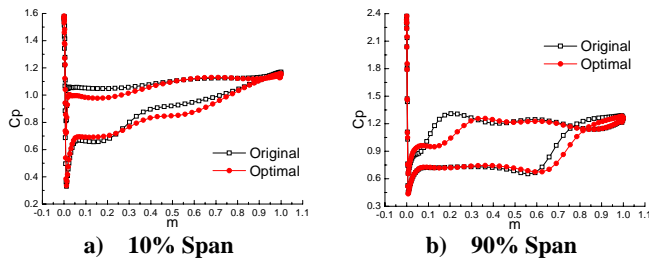


Fig. 11 Comparison of the C_p distributions at the 10%, 90% rotor span at the peak efficiency point

4 MULTISTAGE AXIAL COMPRESSOR OPTIMIZATION

Two double-stage axial fans serve as two optimization examples, Case 1 and Case 2 here. The baseline of Case 1 is an inverse-design-finished two-stage fan (Yang and Shan [18]). As to Case 2, first, on the basis of the optimal configuration of Case 1, the leading edge of Rotor1 is changed to the compound forward-swept one, second, the stacking axis of the compound-swept Rotor1 is adjusted to meet the stress requirement. The above procedures then form the baseline of Case 2. Figure 12 gives the comparison of the two cases. In the two double-stage fan optimization cases, the design before

optimization refers to the original design, and the design after optimization refers to the result in which the 1st stage optimization and the following 2nd stage optimization have both been finished.

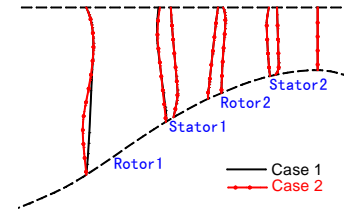


Fig. 12 Comparison of the meridional contours of the two double-stage axial fans in Case 1 and Case 2

4.1 Case 1

4.1.1 Description of the Case

The main geometrical and design specifications of the two-stage fan are listed in Table 2. The comparison of \dot{m} , π and η at the design point between the original design and the design specifications is reported in Table 3. As seen, the CFD-simulated \dot{m} of the original design is about 2% smaller than that of the design specification, which is far beyond the design limitation $\pm 0.5\%$ and leaves the main problem of the original design.

This optimization case took a 100% speed off-design point, the near choked flow point of the original design with a higher total pressure ratio as the optimization condition (see Table 3). The optimization objective was to achieve the maximum mass flow rate of the fan. The work distributions $c_u r$ on computing stations in the through-flow design were chosen as the design variables, while $c_u r$ at LE and TE of four blades kept unchanged. Considering at the design point there were great differences of the total pressure ratio and efficiency between the original design and the design specifications, the optimization constraints here were that π was in between the CFD-simulated original design value near the choked point and the design specification, and η was higher than the CFD-simulated original design value near the choked point. I_{\max} was set to 40.

Table 2 The basic parameters of the two-stage axial fan

	Geometrical Specifications			
	Rotor1	Stator1	Rotor2	Stator2
Inlet hub/tip radius ratio	0.298	0.540	0.642	0.718
Number of blades	18	35	31	49
	Design Specifications			
	U_{tip} m/s	\dot{m} /area kg/(m ² s) (Frontal, Annular)	Φ	
456.0	197.1, 216.4	0.457		
π	τ	Ω		
(Stage1, Stage2)	(Rotor1, Rotor2)	(Stage1, Stage2)		
1.848, 1.600	0.287, 0.253	0.332, 0.653		

4.1.2 Optimization Process

Figure 13 reports the optimization process of the 1st stage optimization for the maximization of the two-stage fan mass flow rate. The three lines in Fig. 13 have the similar meanings to those in Fig. 8 except that their values here correspond to \dot{m} . The six lines in Fig. 14 separately correspond to RMSE of three outputs \dot{m} , π , η of the ANN model after GA and BP optimizing the ANN weights in the 1st stage optimization. The values of RMSE of the training ANN model are about up to 10^{-6} . So the ANN model trained by the hybrid optimization algorithm based on GA and BP has the acceptable approximation fidelity.

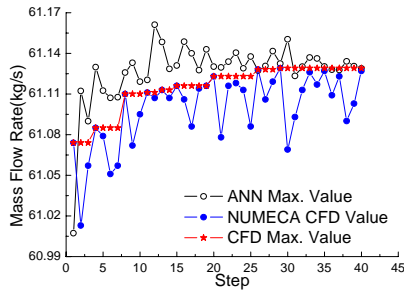


Fig. 13 The 1st stage optimization process for the maximization of the two-stage fan mass flow rate

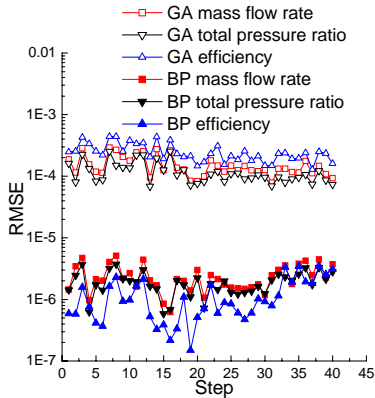


Fig. 14 The root mean square error of the 1st stage optimization for the maximization of the mass flow rate

4.1.3 Results and Analysis

Figure 15 reports the comparison of the 1st, 4th, 8th, 11th element $c_u r$ curves from hub to tip of all the four blade rows in the through-flow design before and after optimization. The $c_u r$ curves of all blades tend to be more concave. The comparison of the radial projections of the hub, middle, tip element airfoils of the two-stage fan blades before and after optimization is shown in Fig. 16. The hub airfoils of rotors and the hub, middle, tip ones of stators change relatively obviously. In order to match with the mass flow rate increase, the values of β_{b2} at Rotor1 hub, β_{b1} and β_{b2} at Rotor2 hub, β_{b1} and β_{b2} at the whole span of Stator1, β_{b1} at the whole span of Stator2 decrease separately.

The comparison of the fan performances before and after

optimization is reported in Table 3. As seen, the fan \dot{m} after optimization at the design point increases to 61.373kg/s, which is 0.12% smaller than the design specification and within the limitation of the latter. Furthermore, η gains 1.2 percentage points, and π changes little in fact. But there are still some differences of π and η with the design specifications. Figure 17 shows the comparison of the fan 100% speed performances before and after optimization. The choked \dot{m} increases noticeably.

Figure 18 reports the comparison of the relative flow angles at inlet and the dimensionless ρ_z at outlet along the span of the fan. The absolute values of the relative flow angles at inlet decrease along the whole span after optimization. Because the flow at inlet is along the axial direction, it is knowable that c_z of the whole span increases. Namely \dot{m} increases. The mass flow rate at outlet obviously increases below the 20% span and up the 70% span after optimization.

Figure 19 shows the comparison of the relative Mach number contours at the 50% span of the fan at the design point before and after optimization. Shocks on the pressure and suction surfaces of Rotor1 and Rotor2 weaken, but the shock on the suction surface of Stator1 becomes stronger. The comparison of the C_p distributions at the 90%, 50%, 10% span of two rotors at the design point is reported in Fig. 20. The C_p distributions on the pressure and suction surfaces of blades are smoother than those before optimization. Shocks on the pressure and suction surfaces at the 50% span and on the pressure surface at the 90% span of Rotor1 weaken obviously. Shocks on the pressure and suction surfaces at the 10% span and on the pressure surface at the 50% span of Rotor2 also weaken obviously. Figure 21 shows the comparison of the streamlines near the suction surfaces of all blades at the design point before and after optimization. As seen, the shock-boundary-layer interference flow separation on the suction surfaces of both Rotor1 and Rotor2 reduces obviously. The flow separation below the 50% span near the trailing edge on the suction surfaces of both Stator1 and Stator2 also reduces obviously. So the weakness of the shock and the reduction of the flow separation should be of benefit to the increase of the mass flow rate.

Table 3 Comparison of fan performances before and after optimization

	Optimization condition	Design point		
	\dot{m} (kg/s)	\dot{m} (kg/s)	π	η
Design specification		61.444	2.957	0.880
Origin	60.259	60.228	2.756	0.853
1 st stage optimization	61.127	61.104	2.763	0.858
2 nd stage optimization	61.400	61.373	2.752	0.865

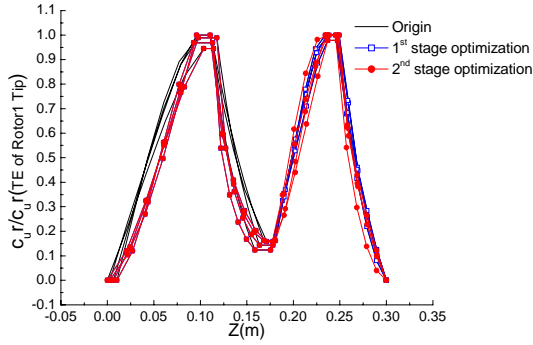


Fig. 15 Comparison of the dimensionless $c_u r$ distribution curves of all the four blade rows in the through-flow design

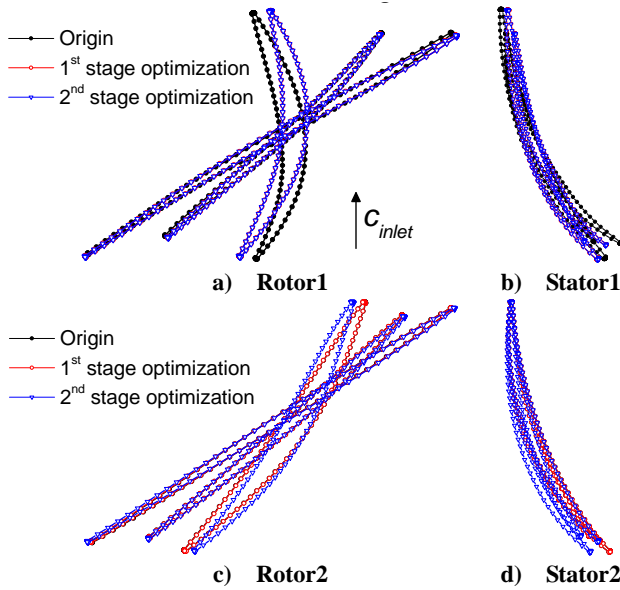


Fig. 16 Comparison of the hub, middle, tip element airfoils of the two-stage fan blades

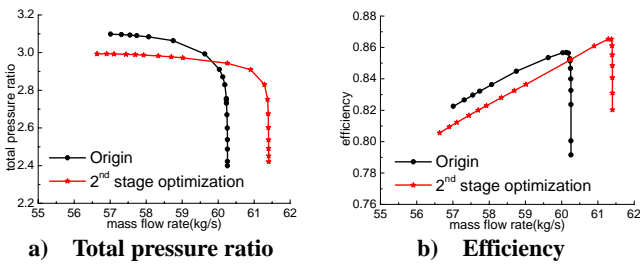


Fig. 17 The fan 100% speed performances

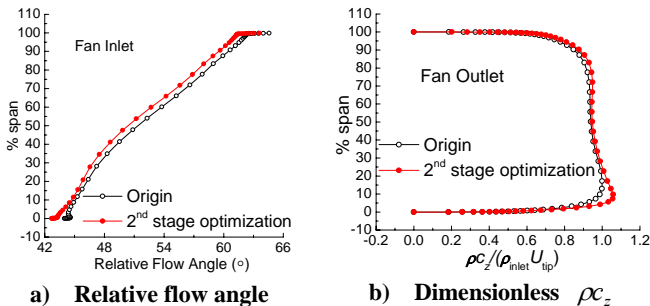


Fig. 18 Comparison of the relative flow angles at inlet and the dimensionless ρc_z at outlet along the span of the fan

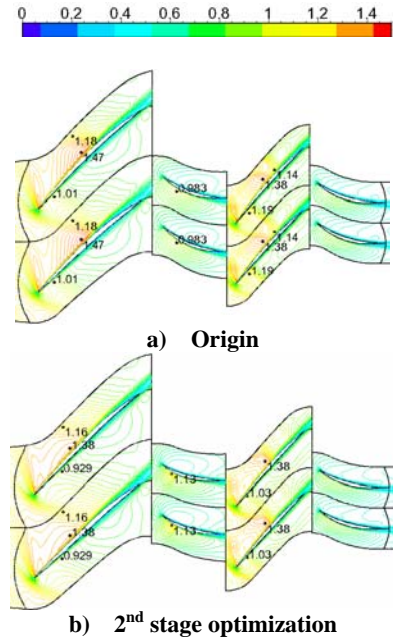


Fig. 19 Comparison of the relative Mach number contours at the 50% span at the design point

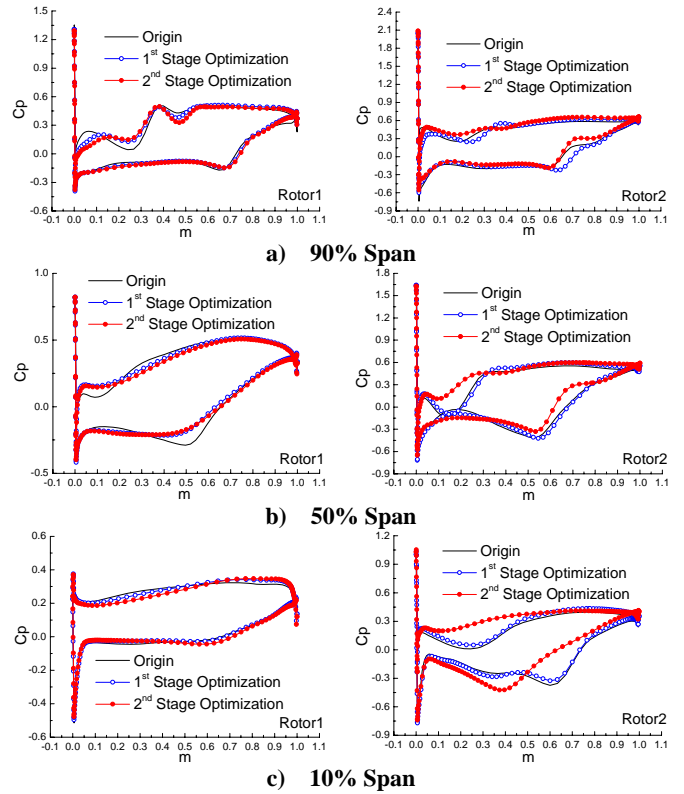
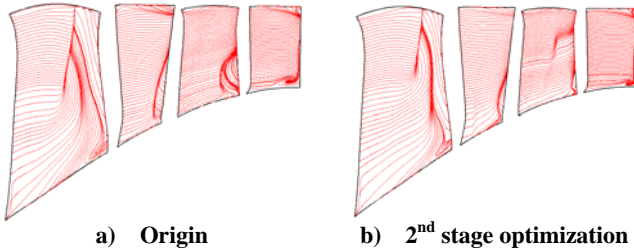


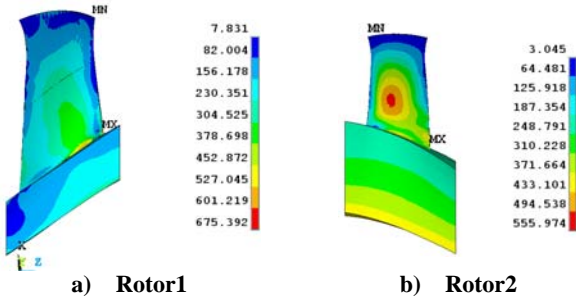
Fig. 20 Comparison of the C_p distributions of two rotors at the 90%, 50%, 10% span at the design point



a) Origin b) 2nd stage optimization
Fig. 21 Comparison of the streamlines near the suction surfaces at the design point

4.1.4 Stress Analysis

The basic constraint for a practical turbomachinery optimization is that blades meet their stress requirements. To focus on at first the strategy problems in the state of the art of the aerodynamic optimization techniques with a smaller computation load, this paper takes no multidisciplinary optimization methodology. Reasonably it takes the simplest method of stress examination. After aero-optimization, a software ANSYS is implemented to analyze the stresses of two rotors which employ the titanium alloy TC11. Figure 22 reports the SEQV distributions of the aerodynamically optimized Rotor1 and Rotor2. Their maximum SEQV values are 675.4MPa and 556.0MPa separately, and the values locate both on the smaller root fillets. It concludes that the optimization techniques used in Case 1 do not destroy the stress states of the two rotors.



a) Rotor1 b) Rotor2
Fig. 22 The SEQV distributions of the two rotors after optimization

4.2 Case 2

4.2.1 Description of the Case

The baseline fan in Case 2, introduced at the beginning of Section 4, is also called the reformed fan. Case 2 has the same design specifications as Case 1 (see Table 3). This case took the 100% speed design point as the optimization condition. The optimization objective was to achieve the maximum adiabatic efficiency of the fan. The design variables were still $c_u r$ as in Case 1. As experienced in Case 1, the total pressure ratio changed little indeed when the $c_u r$ values at the LE and TE were fixed. So the optimization constraints in Case 2 were only to keep the difference between the mass flow rate and the design specification in between $\pm 0.5\%$ of the latter. I_{max} was also set to 40.

4.2.2 Optimization Process

Figure 23 reports the optimization process of the 1st stage optimization for the maximization of the two-stage fan efficiency. The three lines in Fig. 23 have the same meanings as those in Fig. 8.

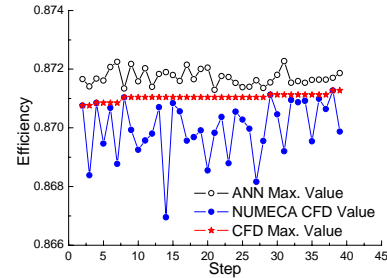


Fig. 23 The 1st stage optimization process for the maximization of the two-stage fan efficiency

4.2.3 Results and Analysis

Figure 24 reports the comparison of the 1st, 4th, 8th, 11th element $c_u r$ curves from hub to tip of all the four blade rows in the through-flow design before and after optimization. The comparison of the radial projections of the hub, middle, tip element airfoils of all the four blades before and after optimization is shown in Fig. 25. After optimization the tip of Rotor1, the hub, middle and tip of both Rotor2 and two stators change obviously. The supersonic precompression airfoils with the S-shape camber lines up the 50% span of the two rotors become more featuring than those before optimization. It contributes to weaken the strength of the rotor passage shock.

The comparison of the fan performances at the design point before and after optimization is reported in Table 4. As seen, after the optimization of efficiency, at the design point, η of the fan gains 0.54 percentage points. \dot{m} is about down by 0.2%, but is still within the limitation of the constraint. As expected, π is not significantly affected. Figure 26 reports the comparison of the fan 100% speed performances before and after optimization. The η values are higher than those of the original design at a wide operation range, and the choked \dot{m} changes little, but the π values at the off-design points reduce some.

Figure 27 reports the comparison of the relative Mach number contours at the 50% span of the fan at the design point before and after optimization. Shocks on the pressure and suction surfaces of Rotor1 and Rotor2, and the shock on the suction surface of Stator1 weaken. The comparison of the C_p distributions at the 90%, 50%, 10% span of Stator1 and Rotor2 at the design point is shown in Fig. 28. The C_p distributions on the pressure and suction surfaces of blades become smoother than those before optimization. Shocks on the suction surface below the 50% span of Stator1 and on the 10% span of Rotor2 weaken. Figure 29 shows the comparison of the streamlines near the suction surface of all blades at the design point before and after optimization. As seen, the shock-boundary-layer interference flow separation on the suction surface of Rotor1

reduces obviously. The flow separation near the TE on the suction surfaces of both Stator1 and Rotor2 reduces some too. So the weakness of the shock and the reduction of the flow separation should be of benefit to the increase of the efficiency.

Table 4 Comparison of fan performances at the design point before and after optimization

	\dot{m} (kg/s)	π	η
Origin of the reformed fan	61.381	2.751	0.8667
1 st stage optimization	61.252	2.748	0.8712
2 nd stage optimization	61.260	2.750	0.8721

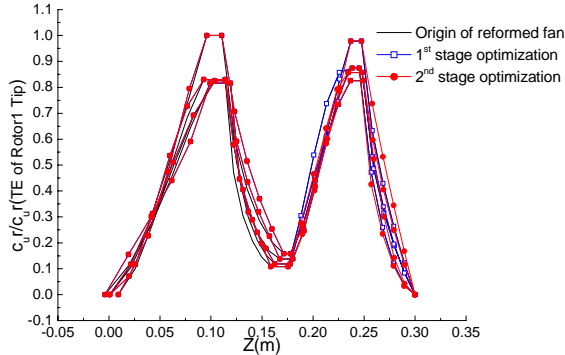


Fig. 24 Comparison of the dimensionless c_u/r distribution curves of all the four blade rows in the through-flow design

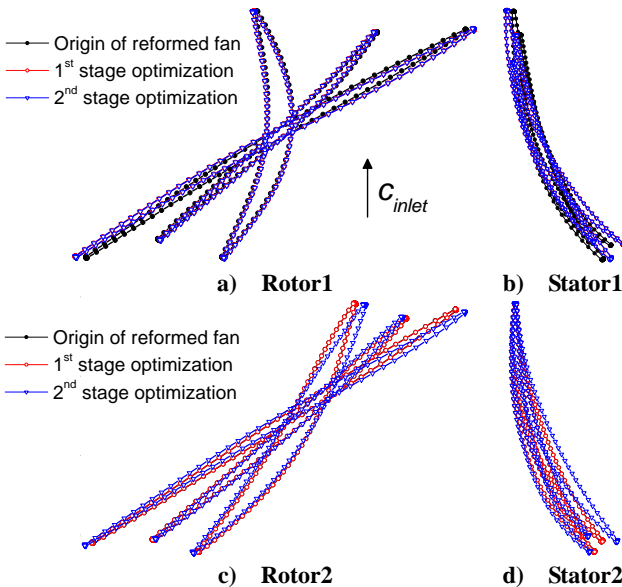


Fig. 25 Comparison of the hub, middle, tip element airfoils of the two-stage fan blades

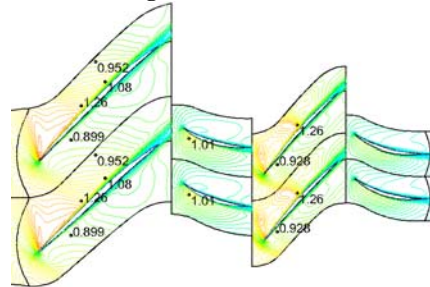
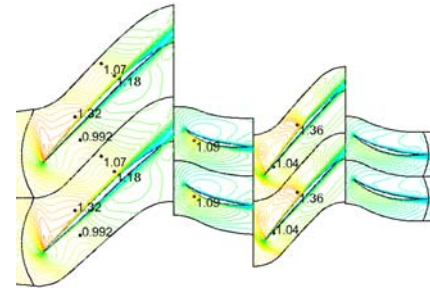
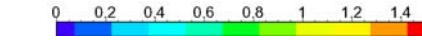
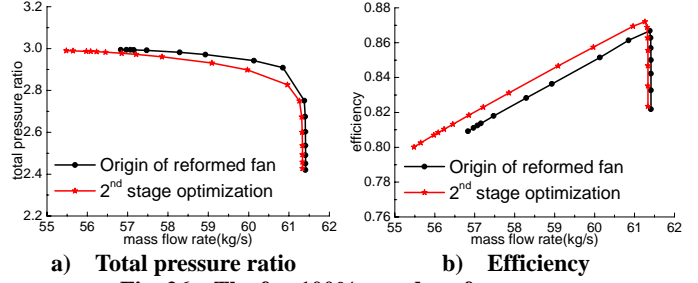
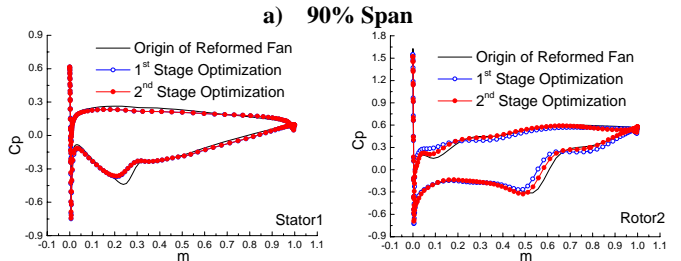
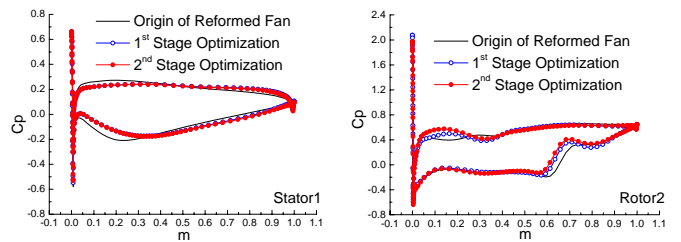


Fig. 27 Comparison of the relative Mach number contours at the 50% span at the design point



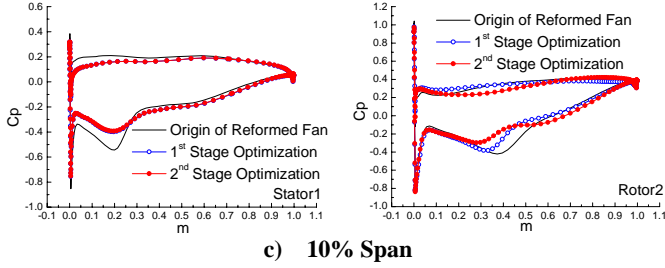


Fig. 28 Comparison of the C_p distributions of Stator1 and Rotor2 at the 90%, 50%, 10% span at the design point

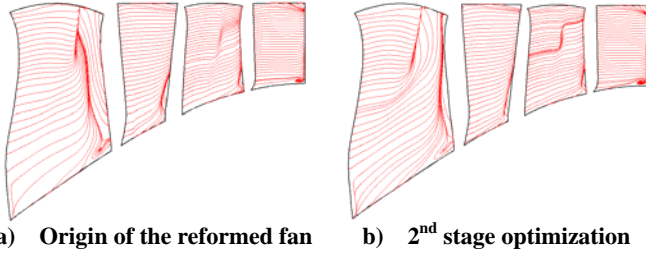


Fig. 29 Comparison of the streamlines near the suction surfaces at the design point

4.2.4 Stress Analysis

After the efficiency optimization the SEQV distributions of two rotors are similar to those in Fig. 22. The maximum SEQV values of Rotor1 and Rotor2 are 722.8MPa and 502.0MPa separately and they are also both on the smaller root fillets. Two rotors after optimization meet their stress requirements.

4.3 Issues and Analyses in Compressor Optimization

The comparison of the C_p distributions at the 10%, 50% span of Stator1 at the design point in Case 1 is reported in Fig. 30. As seen, in Case 1 for the maximization of the fan mass flow rate, although the fan performances become better than those of the original design, there is a stronger shock at the root of Stator1. It is not only to cause a greater shock loss of the stator but also bad for the fan stability. Figure 31 shows the comparison of the hub, middle, tip velocity triangles at the inlet and outlet of Rotor1 before and after optimization of Case 1. In contrast to Fig. 18, the velocity increases at the root between Rotor1 and Stator1, so the gain of the static pressure there drops. Although it makes the adverse pressure gradient at the root of Rotor1 reduce, it causes the strong shock and loss at the root of Stator1. The reason to generate a strong shock there is the automatic over-emphasizing on the maximum of the fan mass flow rate in Case 1. Instead of that, in Case 2 for the maximization of the fan efficiency, the shock at the root of Stator1 weakens obviously.

The comparison of the rotor efficiencies and the stator total pressure recovery coefficients at the design point in Case 1 is listed in Table 5. After the 1st stage optimization, both the Rotor1 η and Stator1 σ increase, while the Rotor2 η reduces. After the 2nd stage optimization, not only the reduction of the Rotor2 η is overcome but also there is some gain. So, in the multistage compressor optimization, although only optimizing a

single stage or even a single row can improve the performance of the integral compressor, it is possible to make some inner components get the mismatching problems when their performances are badly influenced. Namely there is still some room to improve the integral performance of the multistage compressor. According to the above analysis, the suggestions about the multistage compressor optimization are as follows. One should avoid the single blade row optimization as far as possible, apply, from the front to the back, a series of single stage optimizations at least, and had better perform the multistage integral optimization with an effective constraint strategy.

Table 5 Comparison of the rotor η and stator σ at the design point in Case 1

	Rotor1 η	Stator1 σ	Rotor2 η	Stator2 σ
Origin	0.8895	0.9850	0.8927	0.9842
1 st stage optimization	0.9002	0.9856	0.8888	0.9842
2 nd stage optimization	0.9005	0.9861	0.8990	0.9859

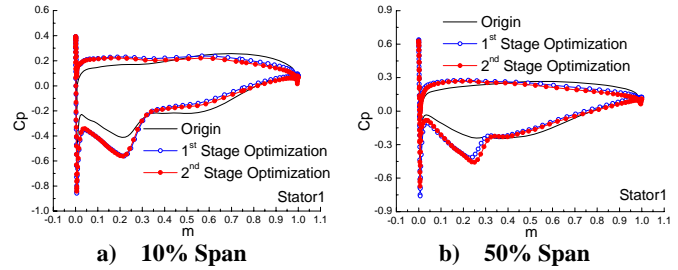


Fig. 30 Comparison of the C_p distributions of Stator1 at the 10%, 50% span at the design point in Case 1

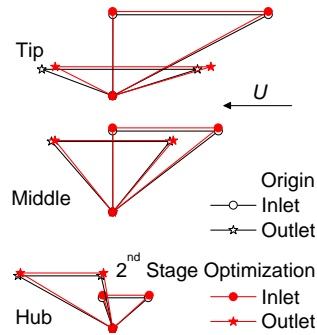


Fig. 31 Comparison of the hub, middle, tip velocity triangles at the inlet and outlet of Rotor1 in Case 1

5 CONCLUSIONS

This paper establishes an optimization platform based on the couple of GA, ANN, inverse design methods and CFD solver. The optimization here mainly has four features. First, it applies conventional inverse design method to parameterize a 3D blade. Such a parameterization method can allow for a direct control of the flow field and the aerodynamic performance. Second, it chooses the aerodynamic parameters with physical meaning as the design variables for the closer correlations between variables and performances. Third, it presents a stage-by-stage

optimization strategy for the multistage compressor in order to reduce the number of variables at the cost of ignoring the influence of the adjacent stages. Fourth, it introduces the visual sensitivity analysis method into the optimization.

In all optimization examples, the design variables are parameterized by means of the Bézier function characterized by being smooth and conveniently controlled. In practice, the control parameters of Bézier curves are used as the optimization variables.

The visual sensitivity analysis reveals the impact of variables on the objective function, resulting in the adjustment of the variation ranges of variables.

This paper applies these techniques to redesign an additional zero-stage rotor and two double-stage fans separately. Choosing the departure angles as the design variables the single rotor optimization increases the efficiency by 0.73 percentage points at the peak efficiency point. In the fan optimization, the work distributions are taken as the design variables. The case of the fan mass flow rate optimization achieves about 1.15kg/s mass flow rate increase together with a efficiency increase of 1.20 percentage points at the design point, and the succeeding case for the fan efficiency optimization gains another efficiency increase of 0.54 percentage points at the design point. The auto-formatting of the precompression airfoil, the shock weakness and the flow separation reduction should be responsible for the improvement of compressor performances. When the optimization emphasizes the increase of the mass flow rate, it is possible to cause a strong shock at the root of the stator. Optimizing only one stage of the multistage compressor is possible to make performances of other components degrade.

It is better to perform the multistage integral optimization under a certain strategy of constraint. It is required that not only to increase the approximation fidelity with more design variables but also to pay attention to the strategy of constraint setting. The complete stage optimization is an unsettled strategy issue, which is how to keep total pressure ratio of the stage unaltered, or increase or decrease it to a newly specified value when changing the work distribution at both the inner passage and the trailing edge of a blade.

ACKNOWLEDGEMENTS

This paper is financed by China Aviation Power Institute and China Gas Turbine Establishment, Aviation Industry Company. The authors would like to thank CAPI and CGTE for the permission to publish this paper.

REFERENCES

- [1] Pierret, S., and Van den Braembussche, R. A., 1999, "Turbomachinery Blade Design Using a Navier-Stokes Solver and Artificial Neural Network," ASME Journal of Turbomachinery, 121, pp. 326-332.
- [2] Chung, J., Shim, J., and Lee, K. D., 2000, "Design of 3D Transonic Compressor Blades Using Numerical Optimization," AIAA Paper No. 2000-0227.
- [3] Kim, J. H., Choi, J. H., and Kim, K. Y., 2009, "Design Optimization of a Centrifugal Compressor Impeller Using Radial Basis Neural Network Method," ASME Paper No. GT2009-59666.
- [4] Bartold, A., and Joos, F., 2008, "Optimization of a Centrifugal Impeller Using Evolutionary Algorithms," ASME Paper No. GT2008-50805.
- [5] Öksüz, Ö., and Akmandor, I. S., 2008, "Axial Turbine Blade Aerodynamic Optimization Using a Novel Multi-Level Genetic Algorithm," ASME Paper No. GT2008-50519.
- [6] Bonaiuti, D., and Zangeneh, M., 2009, "On the Coupling of Inverse Design and Optimization Techniques for the Multiobjective, Multipoint Design of Turbomachinery Blades," ASME Journal of Turbomachinery, 131, pp. 021014-1-021014-16.
- [7] Arabnia, M., and Ghaly, W., 2009, "A Strategy for Multi-Point Shape Optimization of Turbine Stages in Three-Dimensional Flow," ASME Paper No. GT2009-59708.
- [8] Wang, D. X., He, L., Li, Y. S., Wells, R. G., and Chen, T., 2008, "Adjoint Aerodynamic Design Optimization for Blades in Multi-Stage Turbomachines: Part II - Validation and Application," ASME Paper No. GT2008-50209.
- [9] Chen, Z. P., and Yuan, X., 2008, "Aerodynamics Optimum Design of Compressor Blades Based on Numerical Overall Performance Calculation," Journal of Engineering Thermophysics, 29, pp. 221-224 (in Chinese).
- [10] Veress, Á., and Van den Braembussche, R., 2004, "Inverse Design and Optimization of a Return Channel for a Multistage Centrifugal Compressor," Journal of Fluids Engineering, 126, pp. 799-806.
- [11] Chen, B., Gao, X. L., and Yuan, X., 2006, "Aerodynamic 3-Dimensional Optimal Design by NURBS of a Certain Stage Turbine Blades," Journal of Power Engineering, 26, pp. 201-206 (in Chinese).
- [12] Briasco, G., Bruna, D., and Cravero, C., 2008, "A NURBS-Based Optimization Tool for Axial Compressor Cascades at Design and Off-Design Conditions," ASME Paper No. GT2008-50622.
- [13] Chen, N. X., Zhang, H. W., Xu, Q., and Huang, W. G., 2009, "Application of Simple Gradient-Based Method and Multi-Section Blade Parameterization Technique to Aerodynamic Design Optimization of a 3D Transonic Single Rotor Compressor," ASME Paper No. GT2009-59783.
- [14] Verstraete, T., Alsalihi, Z., and Van den Braembussche, R. A., 2007, "Multidisciplinary Optimization of a Radial Compressor for Micro Gas Turbine Applications," ASME Paper No. GT2007-27484.
- [15] Frost, G. R., and Wennerstrom, A. J., 1973, "The Design of Axial Compressor Airfoils Using Arbitrary Camber Lines," ARL 73-0107, AD 765 165.
- [16] Denton, J. D., 1992, "The Calculation of Three-Dimensional Viscous Flow Through Multistage Turbomachines," Journal of Turbomachinery, 114, pp. 18-26.
- [17] Liu, K. H., Shan, P., Li, N., and Zheng, Y., 2006, "Study of Design Method for the Zero-Stage Compressor in an Expendable Gas Turbine Engine," Journal of Aerospace

Power, 21, pp. 1098-1102 (in Chinese).

- [18] Yang, J. J., and Shan, P., 2009, "Design of a High-Loading Two-Stage Forward Swept Fan and Investigation on the Swept-Blading Mechanism," *Journal of Aerospace Power*, 24, pp. 1805-1812 (in Chinese).